Computer Simulation of the Filling Process in Gas-Assisted Injection Molding Based on Gas-Penetration Modeling

Huamin Zhou, Dequn Li

State Key Laboratory of Mold & Die Technology, Huazhong University of Science and Technology, Wuhan, Hubei, 430074, People's Republic of China

Received 22 January 2002; accepted 17 March 2003

ABSTRACT: Gas-assisted injection molding can effectively produce parts free of sink marks in thick sections and free of warpage in long plates. This article concerns the numerical simulation of melt flow and gas penetration during the filling stage in gas-assisted injection molding. By taking the influence of gas penetration on the melt flow as boundary conditions of the melt-filling region, a hybrid finite-element/finite-difference method similar to conventional-injection molding simulation was used in the gas-assisted injection molding-filling simulation. For gas penetration within the gas channel, an analytical formulation of the gas-penetration thickness ratio was deduced based on the matching asymptotic expansion method. Finally, an experiment was employed to verify this proposed simulation scheme and gas-penetration model, by comparing the results of the experiment with the simulation. © 2003 Wiley Periodicals, Inc. J Appl Polym Sci 90: 2377–2384, 2003

Key words: injection molding; interfaces; simulations

INTRODUCTION

Gas-assisted injection molding (GAIM) has become one of the most important multicomponent injection-molding processes in recent years. In gas-assisted injection molding, the mold cavity is partially filled with the polymer melt, followed by the injection of inert gas into the core of the polymer melt. The gas cores out the hot melt at the gap center and forces the melt to fill the whole mold cavity completely (as shown in Fig. 1).[1–4] Compared with conventional injection molding, the required injection and packing pressure is greatly reduced in gas-assisted injection molding. As a result, residual stress and warpage within the molded part can be minimized and the part quality can be improved. It can also avoid sink marks and save material and cycle time because the thickness of the part at the thick sections becomes thinner with the inner gas channel. Gas-assisted injection molding has now accounted for up to 10% of conventional injection molding.[5] Despite the advantages associated with the gas-assisted injection molding process, the molding window and process control become more critical and difficult since additional processes and parameters are involved, including the melt-filled ratio, gas pressure, delay time of gas injection, and gas injection time. The product, tool, and process designs for gas-assisted injection molding are quire complicated and previous experience with conventional injection molding is no longer sufficient. So, computer simulation for gas-assisted injection molding is imperative and is expected to become an important and required tool to help with both part design and process evaluation.

Four distinct regions can be identified during the gas-assisted injection molding filling stage (as shown in Fig. 2): the solidified melt layer close to the mold wall, the deforming viscous melt, the penetration gas, and the unfilled cavity. These four regions are confined by the melt and gas fronts. The melt flow and front in this process is identical to that in conventional mold filling. The gas penetration and its interface are responsible for transmitting the pressure required to move the viscous melt.

For more than a decade, a simulation model based on the Hele–Shaw flow has been being developed to describe the polymer melt flow in thin cavities during conventional injection molding. The typical scheme is finite element/finite difference formulations. These simulations provide acceptable predictions from the engineering application point of view. Now, the existing models meet a new challenge and must be adopted to handle both gas and melt flows in cavities of nonuniform thickness. Although a full-scale three-dimensional analysis may be the final solution, the computational cost is too expensive to be imple-

Correspondence to: H. Zhou (hm-zhou@263.net).

Contract grant sponsor: National Natural Science Foundation Council of the People's Republic of China; contract grant number: 50205011.

Journal of Applied Polymer Science, Vol. 90, 2377–2384 (2003)

mented at the present stage for engineering design purposes.[6–8] At the present stage, adapting simulation algorithms previously developed for conventional injection molding to gas-assisted injection molding based on the similarity of these two processes is more feasible.[9–11] In this method, the melt filling in the thin cavity is assumed as Hele–Shaw flow, and the influence of gas penetration on the melt flow is taken only as boundary conditions of the melt-filling region. Because numerical techniques for a filling simulation of conventional injection molding are well established,[12–15] an additional problem of a gas-assisted injection-molding filling simulation is the solution of the gas-penetration interface. Several attempts used only heat-transfer arguments to set the thickness of the stagnant material behind the advancing gas front.[16,17] Yang[18,19] studied the effect of the dimension of the gas channel on gas penetration. Huzyak and Koelling[20] experimentally studied the isothermal gas penetration of Newtonian melts in circular tubes. Reinelt and Saffman[21] and Blake[22] obtained numerical solutions that are in close agreement with the data for Newtonian melts. Poslinski et al. thoroughly experimented on gas penetration in tubes.[23]

In this article, in considering the characteristics of the filling stage of gas-assisted injection molding, thin film approximation was employed for the polymer melt, and the viscosity of gas and heat transfers in the gas-penetration region were neglected. Thus, a mathematical model governing the behavior of melt flow and gas penetration was established based on the theory of viscous fluid mechanics. In this model, the whole filling region is divided into two regions: the melt-flow region and the gas-penetration region. Melt flow is considered as a Hele–Shaw flow. The pressure and temperature in the gas-penetration region are considered the same everywhere, and the influence of the gas penetration on the melt flow is reflected on the gas-penetration interface. Although numerous investigations have been focused on the gas penetration of gas-assisted injection molding, there is still no reasonable analytical model except for the experiment/experience approaches. Based on the theory of viscous fluid mechanics, a mathematical model governing the behavior of gas penetration was established. Then, a thorough solution by the matching asymptotic expansion method was deduced in detail. Finally, the predicted result by this presented model was compared with experimental observation for verification.

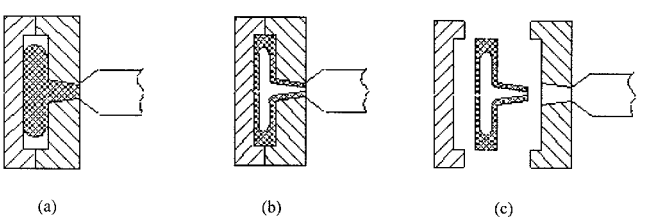

Figure 1 Schematic of gas-assisted injection-molding process: (a) partial polymer melt filling; (b) injection of compressed gas; (c) demolding after packing and cooling.

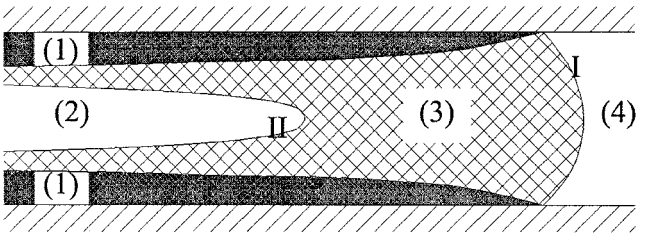

Figure 2 Schematic notation for flow regions and their interface in gas-assisted injection molding: (1) solidified melt layer; (2) penetration gas; (3) deforming viscous melt; (4) unfilled cavity; (I) melt front; (II) gas front.

MODEL OF THE MELT FLOW

According to the characteristics of the filling stage in a thin part, the following assumptions are taken to simplify the formulation: (a) Most injection-molded parts have a thin cavity, and, therefore, the analysis is confined to a relatively thin part such that the flow can be considered to be two-dimensional; (b) because the injection pressure is not very high, the melt is assumed as incompressible; (c) the momentary equation is described by the generalized Hele–Shaw flow, including a quasi-steady approximation due to the thin part and small Reynold number; and (d) heat conduction in the streamwise direction is neglected.

Based on the assumptions above, the relevant governing equations for the continuity, momentum, and energy balance can be described as

$$\frac{\partial(b\bar{u})}{\partial x} + \frac{\partial(b\bar{v})}{\partial y} = 0 \tag{1a}$$

$$\frac{\partial P}{\partial x} - \frac{\partial}{\partial z}\left(\eta \frac{\partial u}{\partial z}\right) = 0 \tag{1b}$$

$$\frac{\partial P}{\partial y} - \frac{\partial}{\partial z}\left(\eta \frac{\partial v}{\partial z}\right) = 0 \tag{1c}$$

$$\rho C_P\left(\frac{\partial T}{\partial t} + u\frac{\partial T}{\partial x} + v\frac{\partial T}{\partial y}\right) = K\frac{\partial^2 T}{\partial z^2} + \eta\left[\left(\frac{\partial u}{\partial x}\right)^2 + \left(\frac{\partial v}{\partial y}\right)^2\right] \tag{1d}$$

where x, y are the planar coordinates in the stream plane and z is the gapwise coordinate with b denoting the half-gap thickness, whereas u, v are the velocity components in the x, y directions, and $\bar{u}$, $\bar{v}$, the averaged whole-gap thickness. In addition, P, T, η, ρ, C_P,

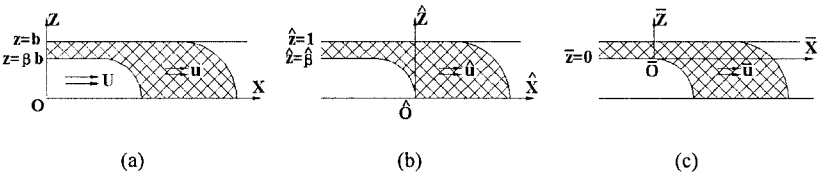

Figure 3 Illustrations of (a) melt flow and gas penetration in the cavity, (b) the outer coordinate system, and (c) the inner coordinate system.

and K are the pressure, temperature, viscosity, density, specific heat, and thermal conductivity of the melt, respectively.

MODEL OF THE GAS FLOW

The velocity of the gas penetration in injection molding is lower than 70 m/s, so the gas can be assumed as incompressible and its viscosity and thermal conductivity can be neglected with respect to the melt. Therefore, the governing equations are

$$P = P(t) \tag{2a}$$

$$T = T(t) \tag{2b}$$

that is, the pressure and temperature of the gas in the cavity is equal everywhere, only varying with the time.

MODELING AND SOLUTION OF GAS PENETRATION

For solving the gas penetration, the governing equations and boundary conditions at the interface are established first. Then, all these equations are transformed to be dimensionless. In the meantime, the capillary number Ca is introduced into the dimensionless equations. The matching asymptotic expansion method is applied to solve these equations. Ca and $Ca^{2/3}$ are used as perturbation parameters to obtain the inner and outer solution of the gas-penetration interface, respectively. By matching these two solutions, the gas-penetration thickness ratio is obtained.

Modeling

Due to obvious reasons, the Hele–Shaw approximation cannot be applied to the gas-penetration interface in the gas channel. As shown in Figure 3(a), suppose that the gas penetrates into the melt in the x direction with the penetration thickness ratio being β. Also, $\vec{n} = n_x\vec{i} + n_y\vec{j} + n_z\vec{k}$ and $\vec{t} = t_x\vec{i} + t_y\vec{j} + t_z\vec{k}$ represent the inner normal and tangent vectors, respectively. The governing equations and boundary conditions in the gas-penetration interface can be simplified as

$$\frac{\partial u}{\partial x} + \frac{\partial w}{\partial z} = 0 \tag{3a}$$

$$-\frac{\partial P}{\partial x} + \eta\left(\frac{\partial^2 u}{\partial x^2} + \frac{\partial^2 u}{\partial z^2}\right) = 0 \tag{3b}$$

$$-\frac{\partial P}{\partial z} + \eta\left(\frac{\partial^2 w}{\partial x^2} + \frac{\partial^2 w}{\partial z^2}\right) = 0 \tag{3c}$$

$$(u - U)n_x + wn_z = 0 \tag{4a}$$

$$\frac{\partial u}{\partial x}\,t_x n_x + \frac{1}{2}\left(\frac{\partial u}{\partial z} + \frac{\partial w}{\partial x}\right)(t_x n_z + t_z n_x) + \frac{\partial w}{\partial z}\,t_z n_z = 0 \tag{4b}$$

$$P - 2\eta\left[\frac{\partial u}{\partial x}\,n_x^2 + \left(\frac{\partial u}{\partial z} + \frac{\partial w}{\partial x}\right)n_x n_z + \frac{\partial w}{\partial z}\,n_z^2\right] = P_0 - \frac{T}{R} \tag{4c}$$

where U is the gas-penetration velocity in the x direction, P_0, T, and R are the pressure of the gas, the melt surface tension coefficient, and the curvature radius of the gas-penetration interface, respectively.

Outer solution

An outer coordinate system for the gas–melt interface is set up as shown in Figure 3(b), and the dimensionless variables in this system are defined by

$$\hat{x} = \frac{x - Ut}{b}; \qquad \hat{z} = \frac{z}{b}; \qquad \hat{R} = \frac{R}{b}; \qquad \hat{u} = \frac{u - U}{U};$$

$$\hat{w} = \frac{w}{U}; \qquad \hat{P} = \frac{P - P_0}{T/b}$$

Based on the variables above, the dimensionless transform of eqs. (3) and (4) results in

$$\frac{\partial u}{\partial x} + \frac{\partial w}{\partial z} = 0 \tag{5a}$$

$$\frac{\partial P}{\partial x} = Ca\left(\frac{\partial^2 u}{\partial x^2} + \frac{\partial^2 u}{\partial z^2}\right) \tag{5b}$$

$$\frac{\partial P}{\partial z} = Ca\left(\frac{\partial^2 w}{\partial x^2} + \frac{\partial^2 w}{\partial z^2}\right) \tag{5c}$$

$$un_x + wn_z = 0 \tag{6a}$$

$$\frac{\partial u}{\partial x} t_x n_x + \frac{1}{2}\left(\frac{\partial u}{\partial z} + \frac{\partial w}{\partial x}\right)(t_x n_z + t_z n_x) + \frac{\partial w}{\partial z} t_z n_z = 0 \tag{6b}$$

$$P - 2Ca\left[\frac{\partial u}{\partial x} n_x^2 + \left(\frac{\partial u}{\partial z} + \frac{\partial w}{\partial x}\right) n_x n_z + \frac{\partial w}{\partial z} n_z^2\right] = -\frac{1}{R} \tag{6c}$$

where Ca is the capillary number and calculated by $Ca = \eta U/T$. For convenience, the superscripts of the variables are removed.

Suppose that the gas-penetration interface is denoted by $z = h(x)$, and, hence, $dz/dx = dh/dx = t_z/t_x = -(n_x/n_z)$. By combining with the boundary conditions, it follows that

$$P = -Ca\left[2\frac{\partial u}{\partial x} + \frac{dh}{dx}\left(\frac{\partial u}{\partial z} + \frac{\partial w}{\partial x}\right)\right] + \frac{d^2 h}{dx^2}\left[1 + \left(\frac{dh}{dx}\right)^2\right]^{-3/2} \tag{7}$$

By adopting Ca as the perturbation parameter and considering the governing equations and the boundary conditions while $Ca \to 0$ with the perturbation theory, the approximation function of h in the outer coordinate system can be obtained as

$$-1 = \frac{d^2 h^0}{dx^2}\left[1 + \left(\frac{dh^0}{dx}\right)^2\right]^{-3/2} \tag{8}$$

By further inference, it results in

$$h^0(x) = \sqrt{1 - (x+1)^2} \tag{9}$$

Equation (9) is the outer solution of the gas-penetration interface.

Inner solution

The point of intersection between the mold wall and the gas-perturbation interface determined by the outer solution is the inconsistent region of the outer solution. This point is selected as the origin to set up the inner coordinate system [as shown in Fig. 3(c)]. In this inner coordinate system, the variables are magnified by δ with $\delta = Ca^m$. To ensure that the magnified equations are in balance and as simple as possible, m is preferred to be 2/3 and

$$\bar{d} = \frac{1-\beta}{\delta}, \quad \bar{x} = \frac{x+1}{\delta^{1/2}}, \quad \bar{z} = \frac{z-1}{\delta}, \quad \bar{h} = \frac{h-1}{\delta}, \quad \bar{u} = u, \quad \bar{w} = \frac{w}{\delta^{1/2}}, \quad \bar{P} = P \tag{10}$$

By substituting eq. (10) into eqs. (5) and (6), the resulting governing equations and boundary conditions in the inner coordinate system can be written as

$$\frac{\partial \bar{u}}{\partial \bar{x}} + \frac{\partial \bar{w}}{\partial \bar{z}} = 0 \tag{11a}$$

$$\frac{\partial \bar{P}}{\partial \bar{x}} = \delta \frac{\partial^2 \bar{u}}{\partial \bar{x}^2} + \frac{\partial^2 \bar{u}}{\partial \bar{z}^2} \tag{11b}$$

$$\frac{\partial \bar{P}}{\partial \bar{z}} = \delta^2 \frac{\partial^2 \bar{w}}{\partial \bar{x}^2} + \delta \frac{\partial^2 \bar{w}}{\partial \bar{z}^2} \tag{11c}$$

$$\bar{w} = \frac{d\bar{h}}{d\bar{x}} \bar{u} \tag{12a}$$

$$\left(\frac{\partial \bar{u}}{\partial \bar{z}} + \delta \frac{\partial \bar{w}}{\partial \bar{x}}\right)\left[1 - \delta\left(\frac{d\bar{h}}{d\bar{x}}\right)^2\right] - 4\delta \frac{\partial \bar{u}}{\partial \bar{x}} \frac{d\bar{h}}{d\bar{x}} = 0 \tag{12b}$$

$$\bar{P} = -2\delta \frac{\partial \bar{u}}{\partial \bar{x}} - \left(\delta \frac{\partial \bar{u}}{\partial \bar{z}} + \delta^2 \frac{\partial \bar{w}}{\partial \bar{x}}\right)\frac{d\bar{h}}{d\bar{x}} + \frac{d^2 \bar{h}}{d\bar{x}^2}\left[1 + \delta\left(\frac{d\bar{h}}{d\bar{x}}\right)^2\right]^{-3/2} \tag{12c}$$

In considering eqs. (11) and (12) while $\delta \to 0$ with the perturbation theory, the approximation function of $\bar{h}$ in the inner coordinate system can be obtained as

$$\frac{\partial^3 \bar{h}^0}{\partial \bar{x}^3} = \frac{-3(\bar{h}^0 + \bar{d})}{(\bar{h}^0)^3} \tag{13}$$

By employing the fourth-order Runge–Kutta method to solve the asymptotic expansion of eq. (13) results in

$$\bar{h}^0(\bar{x}) \approx \frac{A_2 \times 3^{2/3}(\bar{x} + \bar{x}_0)^2}{\bar{d}} + A_1 \times 3^{1/3}(\bar{x} + \bar{x}_0) + A_0 \times \bar{d} + O\left(\frac{1}{\bar{x}}\right) \tag{14}$$

where $A_2 = -0.3215$, $A_1 = -0.096$, and $A_0 = -2.9$. Equation (14) is the inner solution of the gas-penetration interface.

Matching

According to the matching asymptotic expansion theory, the inner solution, when $\bar{x} \to -\infty$, might match the outer solution, when $x \to -1$. This match is satisfied in

any coordinate system, and, here, the outer coordinate system is selected. The inverse transformation to the inner solution according to eq. (10) results in

$$h^0(x) \approx 1 + \frac{A_2 \times 3^{2/3}(x+1)^2}{\bar{d}} + \delta^{1/2}\left(\frac{2 \times A_2 \times 3^{2/3}\bar{x}_0}{\bar{d}} + A_1 \times 3^{1/3}\right)(x+1) + \delta\left(\frac{A_2 \times 3^{2/3}\bar{x}_0^2}{\bar{d}} + A_1 \times 3^{1/3}\bar{x}_0 + A_0 \times \bar{d}\right) + \cdots \quad (15)$$

While $x \to -1$, the outer solution eq. (9) can be expanded as

$$h^0(x) \approx 1 - \frac{1}{2}(x+1)^2 + O[(x+1)^4] \quad (16)$$

Equations (15) and (16) must match each other. Because $(x+1)^n$, all of the $(x+1)^n$ series are linear independent of each other and the coefficients of $(x+1)^n$ of the two solutions should be equivalent. Therefore, $\bar{d}$ can be obtained as

$$\bar{d} = -2A_2 \times 3^{2/3} = 1.3375 \quad (17)$$

Consequently, the gas-penetration thickness ratio in the steady penetration region is calculated by

$$\beta = 1 - \delta\bar{d} = 1 - 1.3375Ca^{2/3} \quad (18)$$

Correction

Equation (18) is the deduced gas-penetration thickness ratio calculating model. Yet, this calculation will lead to a serious deviation when Ca becomes larger. The two reasons are the following: (a) The perturbation method has a close approximation only around the perturbation point. The perturbation parameter Ca was confined by $Ca \to 0$ and $Ca^{2/3} \to 0$ in the deduction process; as a result, the deduced solution is only suitable for small value of Ca. (b) Higher-order items of the asymptotic expansion of the gas-penetration interface solution were neglected, which would lower the accuracy. To make the deduced model applicable to a larger range of Ca, a reasonable correction is needed.

Suppose that the correction function of gas penetration in the outer coordinate system is expressed by

$$h(x) \approx \beta - De^{kx} \quad (19)$$

where D and k are constants that need to be obtained. According to the no slippage condition at the mold wall, the velocity and pressure can be defined by

$$u(x, z) \approx -1 + e^{kx}f_1(z) + O(e^{2kx}) \quad (20a)$$

$$w(x, z) \approx e^{kx}f_2(z) + O(e^{2kx}) \quad (20b)$$

$$P(x, z) \approx Cae^{kx}f_3(z) + O(e^{2kx}) \quad (20c)$$

where f_1, f_2, and f_3 are functions to be solved.

By applying eqs. (19) and (20) to the governing and boundary conditions' equations and expressing f_2 as an assembly of trigonometric functions, the simultaneous equations with respect to all deducible constants can be obtained. Also, these constants will be calculated by solving these equations.

At each time step during the penetration process, the gas-penetration thickness ratio is calculated by eq. (18) first and then corrected by eq. (19). Because the governing and boundary conditions' equations at each penetration position were taken into account in the correction, it will lead to closer approximation in a larger range of Ca.

FILLING SIMULATION

In considering the influence of gas penetration on the melt flow only as boundary conditions of melt-filling region, a hybrid finite-element/finite-difference method is used in the gas-assisted injection-molding filling simulation. In this method, the variables in the flow plane are described in terms of finite elements and the gapwise and time derivatives are expressed by terms of finite difference. The melt-flow front and gas-penetration front are determined by the control volume method.

The simulation process is carried out as follows: First, the flow plane of the cavity and the gas channels

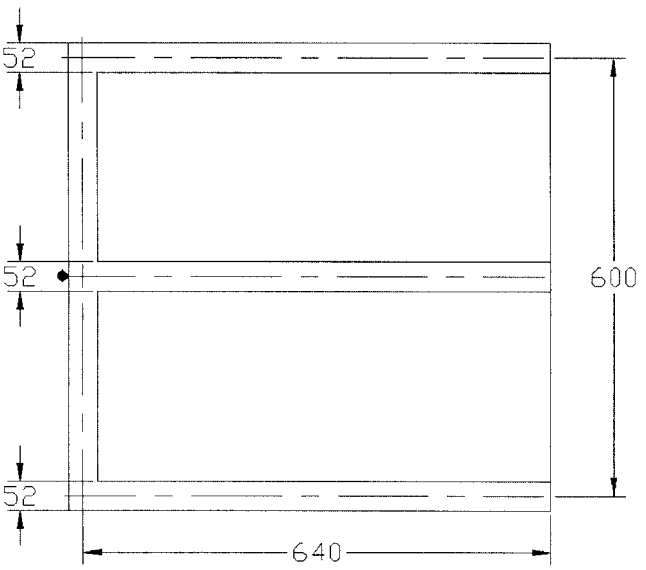

Figure 4 Shape and dimensions of the test part (mm).

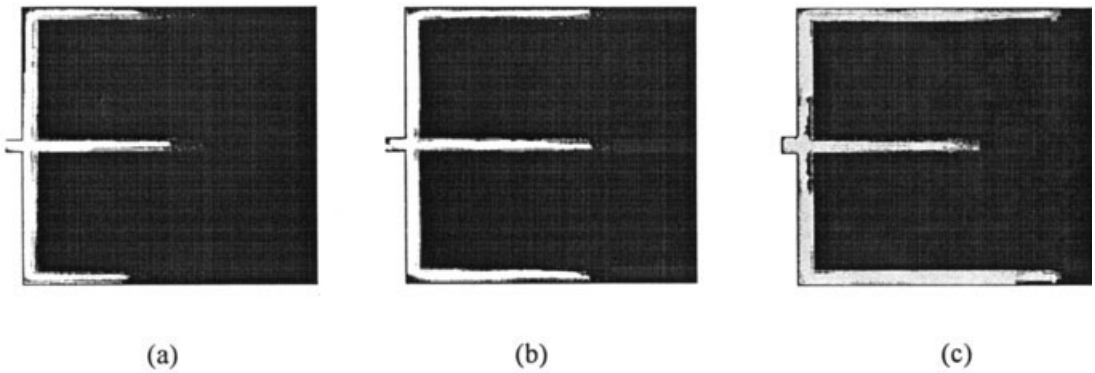

Figure 5 Experimental results with melt-filled ratios of (a) 96%, (b) 92%, and (c) 88%.

is discretized by triangular finite elements with a definite thickness and one-dimensional cylinder elements, respectively, and the triangular finite elements are meshed again with finite-difference grids in the gapwise direction. After meshing, the control volume of each node is calculated. By applying the flow- governing equations to the meshed nodes at the flow plane, the equations with respect to each nodal pressure are deduced. Pressure distribution can be obtained by solving these pressural finite-element equations. Then, the volume flow rate, flow front advancement, shear stress, shear rate, etc., are calculated according to the pressure distribution. In the meantime, the energy equation is applied to all finite-element and finite-difference nodes, and then the nodal temperature at each layer in the gapwise direction is calculated.

After the compressed gas-injection stage begins, the gas pressure is taken as boundary conditions first, and the pressure distribution is solved by iteration calculation of pressure and temperature equations. Then, the gas-penetration velocity is calculated according to the momentum formulation and the pressure gradient at the gas-penetration front. With that, the capillary number and the gas-penetration thickness ratio at that position (i.e., the contact point of the center line of the rib and the gas-penetration interface) are calculated by $Ca = \eta U/T$ and eqs. (18) and (19). With advancement of the gas penetration, the melt viscosity and resistance, the pressure gradient, the cavity size, etc., will change. Thus, the gas-penetration velocity and capillary number will also change. So, the calculation mentioned above must be repeated until the gas cannot penetrate.

VERIFICATION

As shown in Figure 4, the experimental cavity is a plate with three circular ribs with a diameter of 52 mm. The melt and gas-injection gates are both located at the left of the center rib. The selected material is ABS, namely, TFX-250 (HIGH-FLOW). A reequipped Cheng-Shong SM-80 is selected as the molding machine. Also, the major processing conditions are a melt temperature of 200°C, a filling time of 1.0 s, and a pressure-control gas injection with an initial pressure of 25 MPa and a degressive speed of 5 MPa/s. All these conditions are held constant, only changing the melt-filled ratio. Because the ribs are circular, the cored-out section of the gas penetration is annular. After demolding, the molded part is dissected and the skin melt thickness is measured by a screw micrometer, having an accuracy of ± 0.1 mm.

Figures 5–7 illustrate the skin melt thickness results of three cases with different polymer melt-filled ratios of the experiment, the simulation presented in this

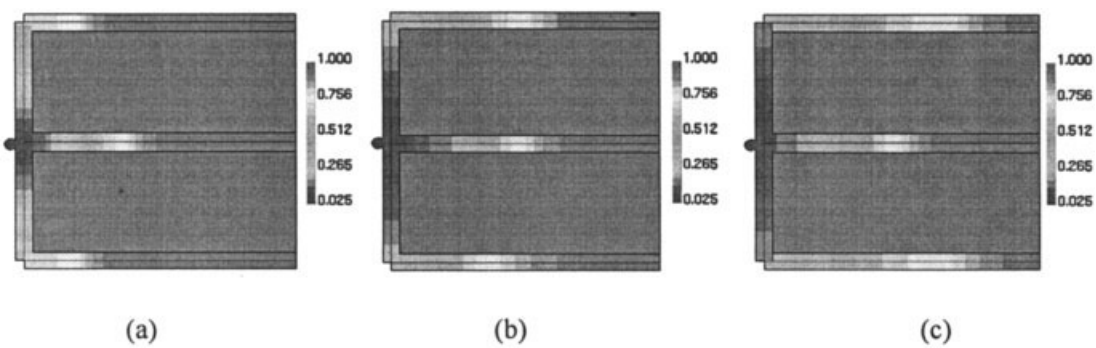

Figure 6 Predications of the presented scheme with melt-filled ratios of (a) 96%, (b) 92%, and (c) 88%.

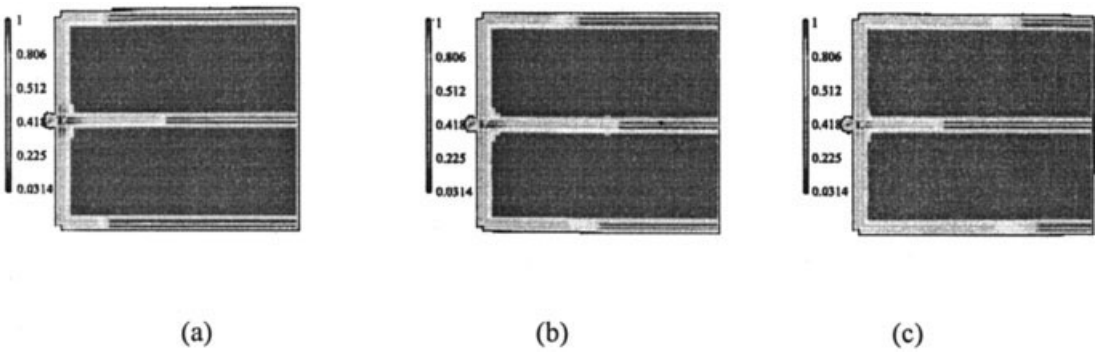

Figure 7 Predications of MF/GAS with melt-filled ratios of (a) 96%, (b) 92%, and (c) 88%.

article, and MF/GAS (the product of Moldflow—the most famous injection-molding simulation corporation), respectively. These comparisons show that (a) the predicted data of the presented scheme are in good agreement with the experimental results and MF/GAS's predications; (b) with the polymer melt-filled ratio decreasing, the predicted gas-penetration extent increases, which conforms to the experiment; and (c) the experiment and two simulations all indicate the same phenomenon: that gas penetration at the top and bottom ribs would catch up with and surpass that at the middle rib with the gas-penetration extent increasing. This is because the middle rib is filled before the other two and, hence, has higher pressure at the polymer-filling stage, so the compression by the gas would be relatively less. The predicted and experimental skin melt thickness ratios of the middle rib are plotted in Figure 8 for comparison. It can be seen that the predicted results based on the proposed model agree well with the experimental data, with the maximum relative deviation being 10.4%.

CONCLUSIONS

Although the filling simulation of gas-assisted injection molding has been studied by many researchers, gas penetration is still a ticklish problem, with the lack of a practical model based on the theory of viscous fluid mechanics. Considering the characteristics of the filling stage of gas-assisted injection molding, a simulation approach was proposed in this article, especially the established theoretical modeling governing the behavior of gas penetration. Also, the solution of the model was conducted by applying the matching asymptotic expansion method. Based on the modeling and solution, a filling simulation system of gas-assisted injection molding named HSCAE/G was developed. The comparison with the experiment and MF/GAS showed that the presented simulation is correct.

The authors would like to acknowledge financial support from the National Natural Science Foundation Council of the People's Republic of China (Grant 50205011).

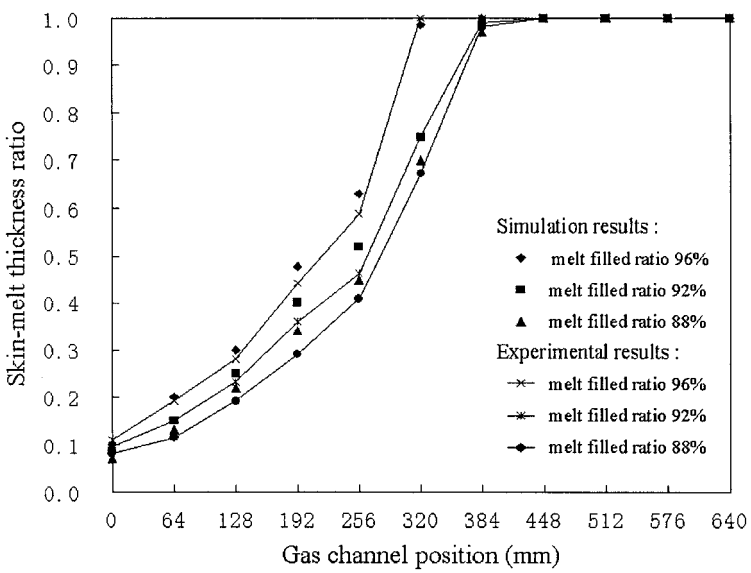

Figure 8 Comparison between experimental skin-melt thickness ratio of the middle rib and the corresponding results of simulation.

References

1. Rusch, K. C. SPE ANTEC Tech Pap 1989, 35, 1014–1018.
2. Shan, S.; Hlavaty, D. Plast Eng 1991, 10, 21–26.
3. Suresh, S. J Inject Mold Technol 1997, 1, 96–103.
4. Wang, K. K.; Nie, Y. Y.; Turng, L. S. Adv Polym Technol 1997, 16, 159–173.
5. Michaeli, W.; Haberstroh, E. Kunststoffe Plast Eur 2000, 90, 52–56.
6. Yang, S. Y.; Liou, S. J.; Liou, W. N. Adv Polym Technol 1997, 16, 175–183.
7. Haagh, G. A. A. V.; Peters, G. W. M.; Van De Vosse, F. N.; Meijer, H. E. H. Polym Eng Sci 2001, 41, 449–465.
8. Khayat, R. E.; Plaskos, C.; Genouvrier, D. Int J Num Methods Eng 2001, 50, 1347–1368.
9. Chen, S. C.; Cheng, N.-T.; Hu, S.-Y. J Appl Polym Sci 1998, 67, 1553–1564.
10. Chung, C. S.; Fu, H. K.; Sheng, H. K. Int J Heat Mass Transfer 1996, 39, 2957–2968.
11. Barton, Stewart, Dandy, Leray, T. J Inject Mold Technol 1997, 1, 104–111.
12. Chiang, H. H.; Hieber, C. A.; Wang, K. K. Polym Eng Sci 1991, 31, 116–124.
13. Chiang, H. H.; Hieber, C. A.; Wang, K. K. Polym Eng Sci 1991, 31, 125–139.
14. Zhou, H.; Li, D. Adv Polym Technol 2001, 20, 125–131.
15. Zhou, H.; Zhang, Y.; Li, D. J Inject Mold Technol 2001, 5, 31–37.
16. Khayat, R. E.; Derdouri, A.; Hebert, L. P. J Non-Newtonian Fluid Mech 1995, 57, 253–270.
17. Chen, S. C.; Hsu, K. F.; Hsu, K. S. J Appl Polym Sci 1995, 58, 793–799.
18. Yang, S. Y.; Liou, S. J. Adv Polym Technol 1995, 14, 197–205.
19. Yang, S. Y.; Huang, F. Z.; Liau, W. N. Polym Eng Sci 1996, 36, 2824–2831.
20. Huzyak, P. C.; Koelling, K. W. J Non-Newtonian Fluid Mech 1997, 71, 73–88.
21. Reinelt, D. A.; Saffman, P. G. SIAM J Sci Stat Comput 1985, 6, 542–561.
22. Blake, K. W.; Ramon, L. C. Chem Eng Sci 1991, 46, 2181–2195.
23. Poslinski, A. J.; Oehler, P. R.; Stokes, V. K. Polym Eng Sci 1995, 35, 877–892.